

Relationship between disorder, magnetism and band topology in $Mn(Sb_{1-x}Bi_x)_2Te_4$ single crystals

Ming Xi(席明) and Hechang Lei(雷和畅)

Citation: Chin. Phys. B, 2024, 33 (**6**): 067503. DOI: 10.1088/1674-1056/ad3dd8
Journal homepage: http://cpb.iphy.ac.cn; http://iopscience.iop.org/cpb

What follows is a list of articles you may be interested in

Effect of In doping on the evolution of microstructure, magnetic properties and corrosion resistance of NdFeB magnets

Yuhao Li(李豫豪), Xiaodong Fan(范晓东), Zhi Jia(贾智), Lu Fan(范璐), Guangfei Ding(丁广飞), Xincai Liu(刘新才), Shuai Guo(郭帅), Bo Zheng(郑波), Shuai Cao(曹帅), Renjie Chen(陈仁杰), and Aru Yan(闫阿儒)
Chin. Phys. B, 2024, 33 (**3**): 037508. DOI: 10.1088/1674-1056/ad0e5c

Enhanced resonance frequency in Co_2FeAl thin film with different thicknesses grown on flexible graphene substrate

Cai Zhou(周偲), Shaokang Yuan(袁少康), Dengyu Zhu(朱登玉), Yuming Bai(白宇明), Tao Wang(王韬), Fufu Liu(刘福福), Lulu Pan(潘禄禄), Cunfang Feng(冯存芳), Bohan Zhang(张博涵), Daping He(何大平), and Shengxiang Wang(汪胜祥)
Chin. Phys. B, 2024, 33 (**3**): 037506. DOI: 10.1088/1674-1056/acfafa

Mechanical and magnetocaloric adjustable properties of Fe_3O_4/PET deformed nanoparticle film

Fengguo Fan(范凤国) and Lintong Duan(段林彤)
Chin. Phys. B, 2024, 33 (**3**): 037502. DOI: 10.1088/1674-1056/acf280

Effect of CeO_2 doping on the coercivity of 2:17 type SmCo magnets

Xiao-Lei Gao(高晓磊), Zhuang Liu(刘壮), Guang-Qing Wang(王广庆), Chao-Qun Zhu(竺超群), Wen-Xin Cheng(程文鑫), Ming-Xiao Zhang(张明晓), Xin-Cai Liu(刘新才), Ren-Jie Chen(陈仁杰), and A-Ru Yan(闫阿儒)
Chin. Phys. B, 2023, 32 (**9**): 097504. DOI: 10.1088/1674-1056/acaa24

Improvement of the microstructure and magnetic properties of (La,Ce)-Fe-B nanocrystalline ribbons

Li-Yu Lian(连李昱), Xiao-Wei Zhang(张晓伟), Ying Liu(刘颖), Jun Li(李军), and Ren-Quan Wang(王仁全)
Chin. Phys. B, 2023, 32 (**7**): 077501. DOI: 10.1088/1674-1056/acd8ae

---

RAPID COMMUNICATION

Relationship between disorder, magnetism and band topology in $Mn(Sb_{1-x}Bi_x)_2Te_4$ single crystals

Ming Xi(席明)[1,2] and Hechang Lei(雷和畅)[1,2,†]

[1] *Department of Physics and Beijing Key Laboratory of Opto-electronic Functional Materials & Micro-nano Devices, Renmin University of China, Beijing* 100872, *China*

[2] *Key Laboratory of Quantum State Construction and Manipulation (Ministry of Education), Renmin University of China, Beijing* 100872, *China*

(Received 18 March 2024; revised manuscript received 6 April 2024; accepted manuscript online 12 April 2024)

We investigate the evolution of magnetic properties as well as the content and distribution of Mn for $Mn(Sb_{1-x}Bi_x)_2Te_4$ single crystals grown by large-temperature-gradient chemical vapor transport method. It is found that the ferromagnetic $MnSb_2Te_4$ changes to antiferromagnetism with Bi doping when $x \geq 0.25$. Further analysis implies that the occupations of Mn ions at Sb/Bi site $Mn_{Sb/Bi}$ and Mn site Mn_{Mn} have a strong influence on the magnetic ground states of these systems. With the decrease of Mn_{Mn} and increase of $Mn_{Sb/Bi}$, the system will favor the ferromagnetic ground state. In addition, the rapid decrease of $T_{C/N}$ with increasing Bi content when $x \leq 0.25$ and the insensitivity of T_N to x when $x > 0.25$ suggest that the main magnetic interaction may change from the Ruderman–Kittel–Kasuya–Yosida type at low Bi doping region to the van-Vleck type in high Bi doped samples.

Keywords: magnetic topological insulator, magnetic properties, antisite defects, chemical vapor transport

PACS: 75.50.Ee, 61.82.Ms, 75.50.Cc, 72.80.Ga **DOI:** 10.1088/1674-1056/ad3dd8

1. Introduction

Topological insulators (TIs) have potential applications in low-energy spintronics because the existence of time-reversal-symmetry-protected surface states and the features of spin and momentum locking with prohibited backscattering of non-magnetic impurities.[1–4] More important, when the magnetism is introduced into TIs, the interplay between magnetic interaction and band topology can lead to the even richer low-dimensional quantum effects, such as quantum anomalous Hall effect (QAHE) in Cr doped (Bi, Sb)$_2$Te$_3$.[5] But the nature of inhomogeneity and the existence of strong disorders in magnetic elements doped TIs impede the exploration of related emergent phenomena and their development as platforms for topological devices. The discovery of intrinsic magnetic topological insulators (MTIs) $MnBi_2Te_4$·$(Bi_2Te_3)_n$ (n = 0–3) family with broken time reversal symmetry and gapped surface state paves a novel way to solve these problems.[6–8] For example, the QAHE can be realized in $MnBi_2Te_4$ at $\sim$ 1.4 K and $MnBi_{10}Te_{16}$ at $\sim$ 1.9 K,[9,10] which are higher than that in Cr doped (Bi, Sb)$_2$Te$_3$.[5] Moreover, these intrinsic MTIs also become a new platform for discovering exotic low-dimensional quantum effects, such as the anion insulator state observed in even layer $MnBi_2Te_4$.[11]

When compared to the intensively studied intrinsic antiferromagnetic TI $MnBi_2Te_4$, the isostructural $MnSb_2Te_4$ grown by different growth methods can exhibit either antiferromagnetic (AFM) or ferromagnetic (FM) ground state, which can be ascribed to the different antisite defects of $Mn_{Sb/Bi}$ and Mn content at Mn site Mn_{Mn}.[12] Furthermore, for $Mn(Sb_{1-x}Bi_x)_2Te_4$ single crystals grown by self-flux method, they exhibit AFM ground state in the whole doping range,[13–18] but for $Mn(Sb_{0.76}Bi_{0.24})_2Te_4$ single crystal grown by chemical vapor transport (CVT) method, it shows ferromagnetism at low temperature.[19] In order to understand the influences of different growth methods on properties of $Mn(Sb_{1-x}Bi_x)_2Te_4$, in the present work, we carried out a detailed study on the evolution of magnetism in CVT-grown $Mn(Sb_{1-x}Bi_x)_2Te_4$ single crystals and analyze the relationships between disorder, magnetism and band topology in these materials.

2. Experimental details

$Mn(Sb_{1-x}Bi_x)_2Te_4$ (x = 0–0.53) crystals were grown by the CVT method. A stoichiometric mixture of the Mn piece (99.99%), Sb grain (99.9999%), Bi grain (99.9999%), and Te lump (99.9999%) was sealed in an evacuated quartz tube with I_2 as the transport agent (about 20 mg·cm^{-3}). The quartz tube was then placed in a two-temperature-zone horizontal furnace and the temperatures of the two zones were raised slowly to 973 K–966 K and 823 K–816 K for 24 h and were then held there for 6 days. Finally, the ampoule was cooled down to room temperature naturally. $Mn(Sb_{1-x}Bi_x)_2Te_4$ single crystals with silvery metallic luster can be obtained from the growth. X-ray diffraction (XRD) patterns were measured using a Bruker D8 x-ray machine with Cu K_α (λ = 1.5418 Å) radiation at room temperature. The elemental analysis was per-

†Corresponding author. E-mail: hlei@ruc.edu.cn

© 2024 Chinese Physical Society and IOP Publishing Ltd

formed using an energy-dispersive x-ray spectroscopy (EDX) analysis. Magnetization measurements were performed in a Quantum Design MPMS-3.

3. Results and discussion

Figure 1(a) shows the crystal structure of $Mn(Sb_{1-x}Bi_x)_2Te_4$ with Mn and Sb/Bi antisite defects. $Mn(Sb_{1-x}Bi_x)_2Te_4$ is isostructural to $MnSb_2Te_4$.[13] The basic two-dimensional (2D) unit of $Mn(Sb_{1-x}Bi_x)_2Te_4$ is the septuple-layer structure of Te–Sb/Bi–Te–Mn–Te–Sb/Bi–Te blocking layer. This septuple-layer structure unit stacks along the c axis with weak van der Waals interlayer interaction. Figure 1(b) shows the XRD patterns of $Mn(Sb_{1-x}Bi_x)_2Te_4$ single crystals. All of the diffraction peaks can be indexed well by the indices of the $(00l)$ lattice planes of $MnSb_2Te_4$ crystal.[13] It indicates that the crystal surfaces are parallel to the ab plane and perpendicular to the c axis. The chemical formulas shown in Fig. 1(b) are the actual atomic ratio determined from EDX when setting the content of Te as 4. It can be seen that $Mn(Sb_{1-x}Bi_x)_2Te_4$ single crystals with $x \leq 0.37$ have the Mn content similar to that of $MnSb_2Te_4$ parent compound, and higher than those in $Mn(Sb_{1-x}Bi_x)_2Te_4$ grown by the self-flux method.[15] When $x = 0.53$, however, the Mn content decreases significantly to 0.88. These results indicate that there are obvious defects in $Mn(Sb_{1-x}Bi_x)_2Te_4$ single crystals and the content of Mn varies with the Bi doping.

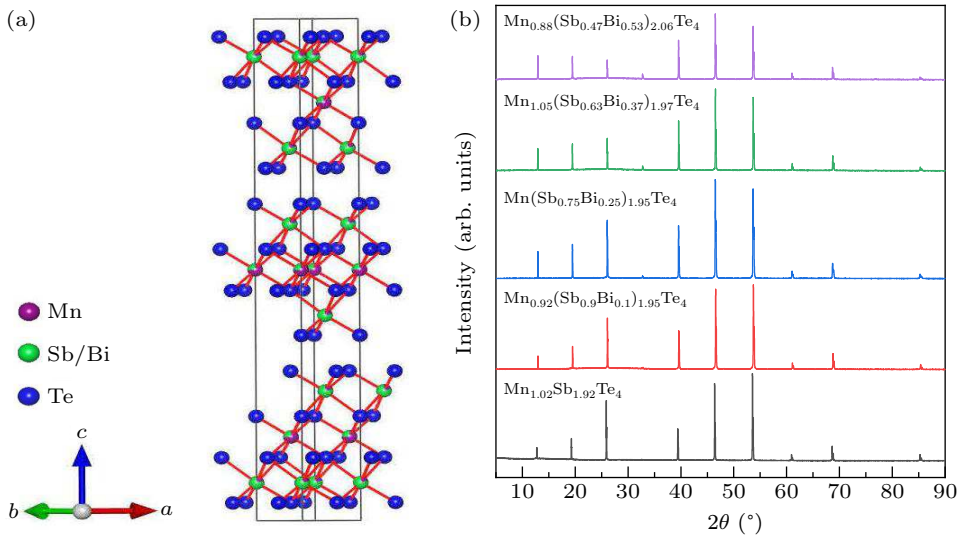


Fig. 1. (a) Crystal structure of $Mn(Sb_{1-x}Bi_x)_2Te_4$ with antisite defects between Mn and Sb/Bi. The purple, green and blue balls represent Mn, Sb/Bi, and Te atoms. (b) XRD patterns of $Mn(Sb_{1-x}Bi_x)_2Te_4$ ($x = 0$–0.53) crystals.

The previous studies have indicated that the content and distribution of Mn have important effects on the magnetic and topological properties of $MnSb_2Te_4$.[12] Thus, we measured the magnetic properties of $Mn(Sb_{1-x}Bi_x)_2Te_4$ crystals in detail. Figures 2(a) and 2(b) exhibit the temperature dependence of magnetic susceptibility $\chi(T)$ for $Mn_{0.92}(Sb_{0.9}Bi_{0.1})_{1.95}Te_4$ single crystal when the field is along the c axis and ab plane, respectively. For both field directions, the $\chi(T)$ curves increase sharply when T is below about 30 K, suggesting a transition from paramagnetism to ferromagnetism. The T_Cs are determined from the temperature corresponding to the peak of the $d\chi/dT$ curves (insets of Figs. 2(a) and 2(b)). The values of T_Cs are 32 K for $H\|c$ and $H\|ab$, which are consistent with each other. It is noted that when $T < T_C$ the value of $\chi(T)$ for $H\|c$ is much larger than that for $H\|ab$, implying that $Mn_{0.92}(Sb_{0.9}Bi_{0.1})_{1.95}Te_4$ is an easy c-axis ferromagnet. In addition, the zero-field-cooling (ZFC) and field-cooling (FC) $\chi(T)$ curves at $\mu_0 H = 0.02$ T for both field directions show the features of bifurcation, which possibly originate from the multi-domain feature in the low-field region. Figures 2(c) and 2(d) show the field dependence of magnetization $M(\mu_0 H)$ at various temperatures for $H\|c$ and $H\|ab$, respectively. The $M(\mu_0 H)$ curves for both field directions at low temperatures exhibit sharp increases in the low-field region, consistent with the $\chi(T)$ curves and further confirming the FM ground state of $Mn_{0.92}(Sb_{0.9}Bi_{0.1})_{1.95}Te_4$. Moreover, there are no obvious hystereses for these curves, implying the soft magnetic characteristics of the $Mn_{0.92}(Sb_{0.9}Bi_{0.1})_{1.95}Te_4$ crystal. At $T = 2$ K the saturation field for $H\|c$ is smaller than that for $H\|ab$, indicating that the easy magnetization direction of $Mn_{0.92}(Sb_{0.9}Bi_{0.1})_{1.95}Te_4$ is along the c axis, consistent with the $\chi(T)$ results. It can be seen that the initial saturation moments M_{is}s of $Mn_{0.92}(Sb_{0.9}Bi_{0.1})_{1.95}Te_4$ single crystal are about 2.24 μ_B/Mn at 5 T for both $H\|c$ and $H\|ab$, which are not only higher than the reported value in $MnSb_2Te_4$ synthesized by CVT method (~ 2.02 μ_B/Mn), but also higher than that of the FM $MnSb_{1.8}Bi_{0.2}Te_4$ (~ 1.8 μ_B/Mn) with similar proportion but lower T_C (~ 26 K) grown by self-flux method.[20] On the other hand, with increasing temperature, the M_{is} at 5 T decreases gradually and the sharp increase of $M(\mu_0 H)$ at low-

field region changes into a S-shape at 35 K, suggesting that $Mn_{0.92}(Sb_{0.9}Bi_{0.1})_{1.95}Te_4$ becomes a paramagnet at that temperature.

In order to further reveal the doping effects of Bi, the temperature dependences of $\chi(T)$ for $Mn(Sb_{1-x}Bi_x)_2Te_4$ ($x = 0$, 0.1, 0.25, 0.37, and 0.53) single crystals when the field is along the c axis are measured, as shown in Figs. 3(a)–3(e). It can be seen that the ground state of $Mn(Sb_{1-x}Bi_x)_2Te_4$ single crystals changes gradually from the FM to AFM with the increase of Bi content, i.e., the samples with $x = 0$ and 0.1 exhibit FM ground states, while the samples with high Bi doping level ($x = 0.25$, 0.37, and 0.53) show AFM ground states. The T_Cs determined from the peak of $d\chi/dT$ curve are 38 K and 32 K for $x = 0$ and $x = 0.1$ crystals. The T_Ns obtained from the temperature corresponding to the peak position of $\chi(T)$ curve are 23.5 K, 24.0 K and 24.3 K for $x = 0.25$, 0.37 and 0.53, respectively. In addition, according to the previous theoretical work about the determination of T_N for the long-range AFM order,[21] the T_N can be determined from the peak of $d(\chi T)/dT$ (insets of Figs. 3(c)–3(e)). It is found that for AFM $Mn(Sb_{1-x}Bi_x)_2Te_4$ ($x = 0.25$, 0.37, 0.53) samples, the AFM transition temperatures determined from the peak positions of $d(\chi T)/dT$ ($T_{N1} = 22.8$ K, 23.3 K and 23.8 K for $x = 0.25$, 0.37 and 0.53) are close to the above values and the T_Ns determined from both methods increase with increasing x consistently. It is reasonable because the transition regions from paramagnetism to antiferromagnetism in $Mn(Sb_{1-x}Bi_x)_2Te_4$ ($x = 0.25$, 0.37, 0.53) samples are narrow. Interestingly, the T_C decreases dramatically with the increase of x when $x < 0.25$, but with increasing x further, the T_N is almost unchanged, i.e., insensitive to the Bi content. As shown in the inset of Fig. 3(f), the field dependences of $M(\mu_0 H)$ of FM $Mn(Sb_{1-x}Bi_x)_2Te_4$ ($x = 0$, 0.1) samples at $T = 2$ K for $H\|c$ in the field range between -1 T and 1 T do not show the obvious hysteresis, indicating the soft magnetic properties of these samples. For AFM $Mn(Sb_{1-x}Bi_x)_2Te_4$ ($x = 0.25$, 0.37 and 0.53) crystals, they exhibit a spin-flop behavior at high field and the initial spin-flop field $\mu_0 H_{sp}$ increases from ~ 0.45 T for $x = 0.25$ sample to ~ 1.75 T for $x = 0.53$ sample (Fig. 3(f)). These $\mu_0 H_{sp}$ are smaller than that ($\mu_0 H_{sp} \sim 3.5$ T) of $MnBi_2Te_4$ grown by CVT and self-flux methods.[15,22]

Figure 4(a) exhibits the initial saturation magnetization M_{is} of $Mn(Sb_{1-x}Bi_x)_2Te_4$ as a function of x. It shows a nearly linear dependence on x between $0 \le x \le 0.53$. It is noted that the M_{is} (~ 3.8 μ_B/Mn) of CVT-grown $MnBi_2Te_4$ crystal[22] is also perfectly consistent with this linear trend, suggesting that the linear x dependence of M_{is} in CVT-grown $Mn(Sb_{1-x}Bi_x)_2Te_4$ crystals should be satisfied in the full solid solution range ($0 \le x \le 1$). In addition, this linear dependence between M_{is} and x also exists in $Mn(Sb_{1-x}Bi_x)_2Te_4$ series grown by self-flux method,[15,16] but all M_{is}s of the samples grown by self-flux method are lower than those of CVT-grown samples with similar compositions.[15,22]

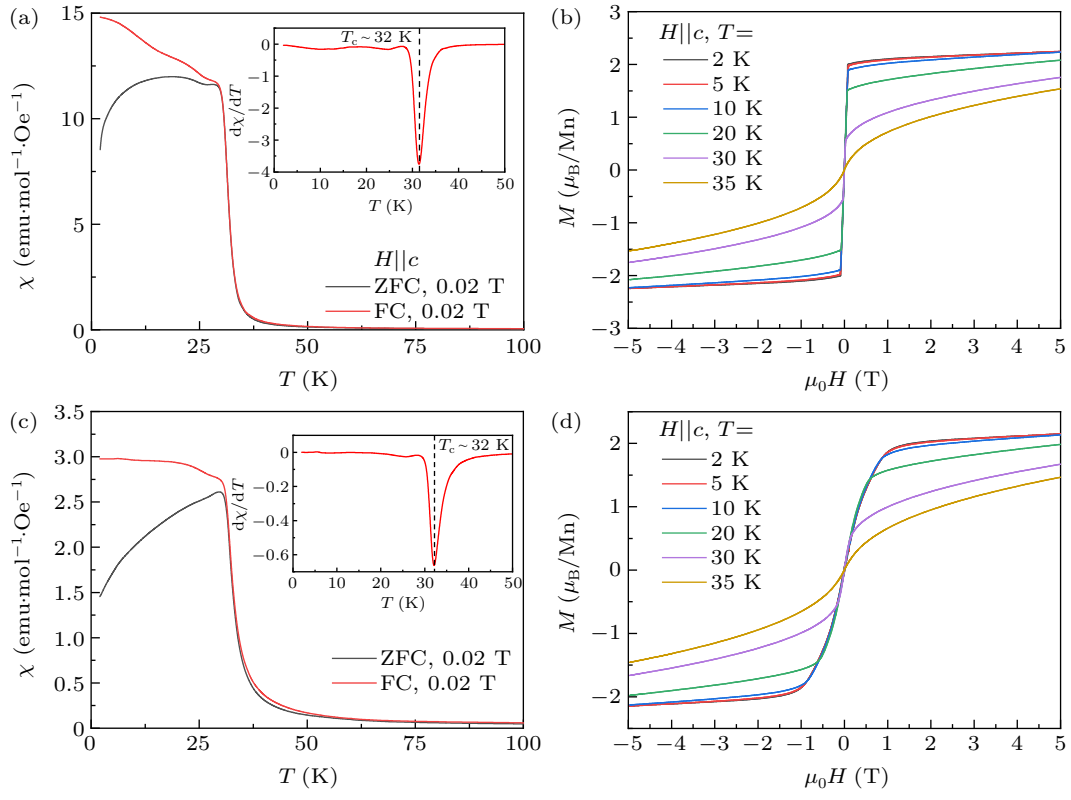


Fig. 2. Magnetic properties of $Mn_{0.92}(Sb_{0.9}Bi_{0.1})_{1.95}Te_4$ single crystal grown by CVT method. (a) and (c) Temperature dependence of $\chi(T)$ at $\mu_0 H = 0.02$ T with ZFC and FC modes for $H\|c$ and $H\|ab$, respectively. The insets show the $d\chi/dT$ as a function of temperature at $T \le 50$ K. (b) and (d) Field dependence of $M(\mu_0 H)$ at different temperatures for $H\|c$ and $H\|ab$, respectively.

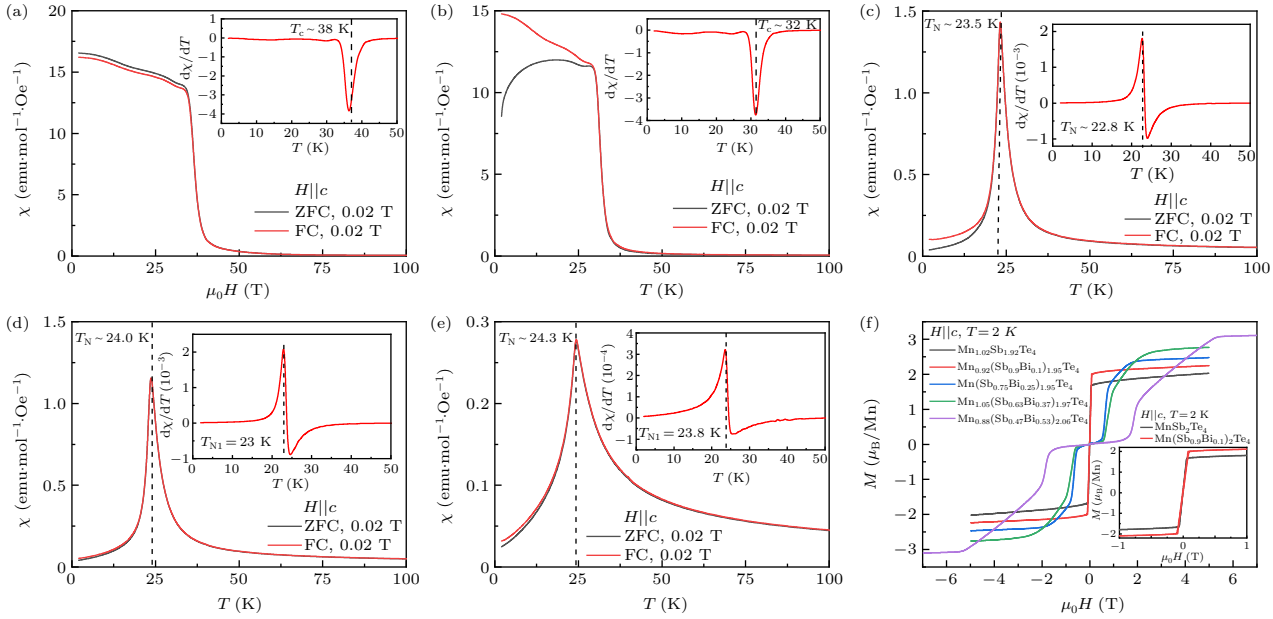


Fig. 3. Magnetic properties of $Mn(Sb_{1-x}Bi_x)_2Te_4$ single crystals. (a)–(e) Temperature dependence of $\chi(T)$ for samples with $x = 0$, 0.1, 0.25, 0.37, and 0.53 at $\mu_0 H = 0.02$ T with ZFC and FC modes for $H\|c$, respectively. The insets in (a) and (b) show the $\mathrm{d}\chi/\mathrm{d}T$ as a function of temperature at $T \leq 50$ K. The insets of (c)–(e) show the $\mathrm{d}(\chi T)/\mathrm{d}T$ as a function of temperature at $T \leq 50$ K of AFM $Mn(Sb_{1-x}Bi_x)_2Te_4$ ($x = 0.25$, 0.37 and 0.53) samples, respectively. The T_{N1}s are determined from the positions of positive peaks. (f) Field dependence of $M(\mu_0 H)$ for samples with $x = 0$, 0.1, 0.25, 0.37, and 0.53 at $T = 2$ K for $H\|c$. The inset shows the field dependence of $M(\mu_0 H)$ of FM $Mn(Sb_{1-x}Bi_x)_2Te_4$ ($x = 0$, 0.1) samples at $T = 2$ K for $H\|c$ in the field range between -1 T and 1 T.

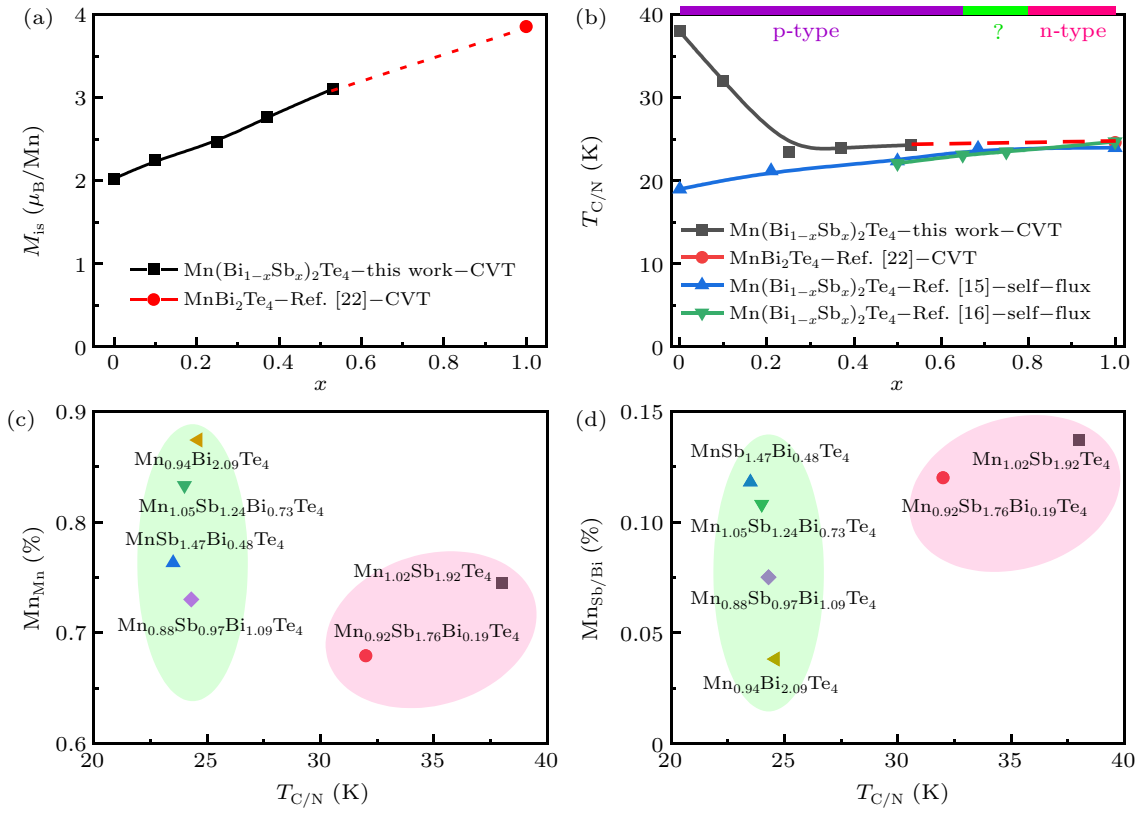


Fig. 4. (a) The M_{is} of $Mn(Sb_{1-x}Bi_x)_2Te_4$ single crystals as a function of x. (b) The dependence of $T_{C/N}$ on x and carrier type for $Mn(Sb_{1-x}Bi_x)_2Te_4$ single crystals obtained by different synthesis methods. (c) and (d) Content of Mn ions at the Mn site (Mn_{Mn}) and Mn ions at the Sb/Bi site ($Mn_{Sb/Bi}$) as a function of $T_{C/N}$ of CVT-grown $Mn(Sb_{1-x}Bi_x)_2Te_4$ single crystals, respectively.

In the Mn–Sb/Bi–Te and magnetic element doped TI systems, there are two main magnetic exchange mechanisms. One is van-Vleck type and the other is Ruderman–Kittel–Kasuya–Yosida (RKKY) type. For the former, it is insensitive to the carrier concentration and type, but strongly related to the strength of spin–orbit coupling (SOC) and band inversion.[23] For the latter, the RKKY-type magnetic exchange interaction depends on the carrier concentration.[20] Figure 4(b) shows

the dependence of $T_{C/N}$ of $Mn(Sb_{1-x}Bi_x)_2Te_4$ obtained by different synthesis methods on x and carrier type. For self-flux grown $Mn(Sb_{1-x}Bi_x)_2Te_4$ samples with $x \geq 0.6$, their T_Ns change slightly with increasing x.[15,16] It suggests that the van-Vleck-type magnetic exchange interaction should be dominant in this region and the RKKY-type interaction only leads to the weak increase of T_N when doping more Bi (large x). Furthermore, the angle-resolved photoemission spectroscopy (ARPES) measurements indicate that the samples in this region have the nontrivial band topology, consistent with the dominant van-Vleck type magnetic interaction, because both of them originate from the large SOC-induced band inversion.[20,23] The T_Ns of CVT-grown $Mn(Sb_{1-x}Bi_x)_2Te_4$ samples with $x > 0.25$ also show a similar trend on x, implying that the main magnetic exchange interaction in these samples should be van-Vleck-type and they may have topological nontrivial electronic structures as well. In contrast, the carrier concentration of self-flux grown $Mn(Sb_{1-x}Bi_x)_2Te_4$ samples with $x \leq 0.37$ increases rapidly with the decrease of x,[24] which should lead to the enhanced RKKY-type magnetic interaction. But the T_Ns in this region tend to decrease with lowering Bi content.[15] It strongly suggests that the strength of van-Vleck type magnetic interaction should decrease dramatically, which can be explained by the decrease of SOC and disappearance of band inversion. It is in agreement with the topologically trivial band structure of $MnSb_2Te_4$ observed by the ARPES.[12] On the other hand, for the CVT-grown $Mn(Sb_{1-x}Bi_x)_2Te_4$ samples with $x \leq 0.25$, the $T_{C/N}$ increases significantly with decreasing x. It suggests that the dominant magnetic interaction in these samples should be the RKKY-type because of large carrier concentration when compared to the flux-grown sample in this region.[12,24] Moreover, the ARPES results show that the electronic structure of CVT-grown $MnSb_2Te_4$ is topological trivial and the absence of band inversion should result in the weakening of van-Vleck magnetic interaction.

Via the M_{is} at 5 T for $H \| c$, the effective moment of Mn ions μ_{eff} ($\sim 4.7\ \mu_B$/Mn),[25] and the experiment composition, the contents of Mn_{Mn} and $Mn_{Sb/Bi}$ can be estimated.[25] The relationships between $T_{C/N}$ and Mn_{Mn} as well as $Mn_{Sb/Bi}$ are plotted in Figs. 4(c) and 4(d). It can be seen that the Mn_{Mn} contents of FM $Mn_{0.92}Sb_{1.76}Bi_{0.19}Te_4$ and $Mn_{1.02}Sb_{1.92}Te_4$ (highlighted by pink area) are lower than those in AFM samples with higher Bi contents ($x > 0.1$) in principle (highlighted by green area) when their $Mn_{Sb/Bi}$ contents are higher than the latter. Previous study shows that the occupations of Mn_{Mn} and $Mn_{Sb/Bi}$ have a strong influence on the magnetic ground states of these systems.[15,26] First, the interblock interaction between Mn_{Mn} is AFM intrinsically. Second, the intrablock interaction between Mn_{Mn} and $Mn_{Sb/Bi}$ is also AFM when the interblock $Mn_{Sb/Bi}$ is coupled ferromagnetically.[26] Thus, the higher $Mn_{Sb/Bi}$ in samples with $x \leq 0.1$ could drive the system to the FM ground state. In contrast, the samples with higher Bi content, in which the $Mn_{Sb/Bi}$ are lower, will have an AFM ground state. On the other hand, the relatively low content of Mn_{Mn} for $x \leq 0.1$ samples will reduce the interblock AFM interaction when compared to the $x \geq 0.25$ samples further, i.e., favoring the formation of FM ground state.

4. Conclusion

We develop a large-temperature-gradient CVT method to grow $Mn(Sb_{1-x}Bi_x)_2Te_4$ single crystals. It is found that with Bi doping, the magnetic properties of $Mn(Sb_{1-x}Bi_x)_2Te_4$ change from ferromagnetism to antiferromagnetism when $x \geq 0.25$. It is distinctly different from the flux-grown samples that show the AFM ground state in the whole doping range. Such difference could be ascribed to the different contents of Mn_{Mn} and antisite defects $Mn_{Sb/Bi}$. The lower Mn_{Mn} and higher $Mn_{Sb/Bi}$ contents will tend to form the FM ground state. On the other hand, the rapid decrease of $T_{C/N}$ when $x \leq 0.25$ and the nearly unchanged T_N when $x > 0.25$ imply that the main magnetic interaction is the RKKY type at low Bi doping region, in contrast to the dominant van-Vleck type in high Bi doped samples. It is consistent with the evolution of band topology of $Mn(Sb_{1-x}Bi_x)_2Te_4$ from trivial to nontrival with Bi doping.

Acknowledgments

Project supported by the Beijing Natural Science Foundation (Grant No. Z200005), the National Key R&D Program of China (Grant Nos. 2022YFA1403800 and 2023YFA1406500), the National Natural Science Foundation of China (Grant No. 12274459), and Collaborative Research Project of Laboratory for Materials and Structures, Institute of Innovative Research, Tokyo Institute of Technology.

References

[1] Fu L, Kane C L and Mele E J 2007 *Phys. Rev. Lett.* **98** 106803
[2] Lee W C, Wu C, Arovas D P and Zhang S C 2009 *Phys. Rev. B* **80** 245439
[3] Roushan P, Seo J, Parker C V, Hor Y S, Hsieh D, Qian D, Richardella A, Hasan M Z, Cava R J and Yazdani A 2009 *Nature* **460** 1106
[4] Biswas R R and Balatsky A V 2010 *Phys. Rev. B* **81** 233405
[5] Chang C Z, Zhang J, Feng X, Shen J, Zhang Z, Guo M, Li K, Ou Y, Wei P, Wang L L, Ji Z, Feng Y, Ji S H, Chen X, Jia J F, Dai X, Fang Z, Zhang S C, He K, Wang Y Y, Lu L, Ma X C and Xue Q K 2013 *Science* **340** 167
[6] Otrokov M M, Klimovskikh I I, Bentmann H, *et al.* 2019 *Nature* **576** 416
[7] Yan J Q, Liu Y H, Parker D S, Wu Y, Aczel A A, Matsuda M, McGuire M A and Sales B C 2020 *Phys. Rev. Mater.* **4** 054202
[8] Hu C, Ding L, Gordon K N, Ghosh B, Tien H J, Li H X, Linn A G, Lien S W, Huang C Y, Mackey S, Liu J Y, Singh B, Agarwal A, Bansil A, Song M, Li D S, Xu S Y, Lin H, Cao H B, Chang T R, Dessau D and Ni N 2020 *Sci. Adv.* **6** eaba4275
[9] Deng Y J, Yu Y J, Shi M Z, Guo Z X, Xu Z H, Wang J, Chen X H and Zhang Y B 2020 *Science* **367** 895

[10] Deng H M, Chen Z Y, Wołoś A, Konczykowski M, Sobczak K, Sitnicka J, Fedorchenko I V, Borysiuk J, Heider T, Pluciński Ł, Park K, Georgescu A B, Cano J and Krusin-Elbaum L 2021 *Nat. Phys.* **17** 36
[11] Liu C, Wang Y C, Li H, Wu Y, Li Y X, Li J H, He K, Xu Y, Zhang J S and Wang Y Y 2020 *Nat. Mater.* **19** 522
[12] Xi M, Chen F, Gong C, Tian S, Yin Q, Qian T and Lei H C 2022 *J. Phys. Chem. Lett.* **13** 10897
[13] Liu Y H, Wang L L, Zheng Q, Huang Z L, Wang X P, Chi M F, Wu Y, Chakoumakos B C, McGuire M A, Sales B C, Wu W D and Yan J Q 2021 *Phys. Rev. X* **11** 021033
[14] Wimmer S, Sánchez-Barriga J, Küppers P, Ney A, Schierle E, Freyse F, Caha O, Michalička J, Liebmann M, Primetzhofer D, Hoffman M, Ernst A, Otrokov M M, Bihlmayer G, Weschke E, Lake B, Chulkov E V, Morgenstern M, Bauer G, Springholz G and Rader O 2021 *Adv. Mater.* **33** 2102935
[15] Yan J Q, Okamoto S, McGuire M A, May A F, McQueeney R J and Sales B C 2019 *Phys. Rev. B* **100** 104409
[16] Chen B, Fei F C, Zhang D Q, Zhang B, Liu W L, Zhang S, Wang P D, Wei B Y, Zhang Y, Zuo Z W, Guo J W, Liu Q Q, Wang Z L, Wu X C, Zong J Y, Xie X D, Chen W, Sun Z, Wang S C, Zhang Y, Zhang M H, Wang X F, Song F Q, Zhang H J, Shen D W and Wang B G 2019 *Nat. Commun.* **10** 4469
[17] Pei C Y, Xi M, Wang Q, Shi W J, Gao L L, Zhao Y, Tian S J, Cao W Z, Li C H, Zhang M X, Zhu S H, Chen Y L, Lei H C and Qi Y P 2022 *Phys. Rev. Mater.* **6** L101801
[18] Gao L L, Wu J F, Xi M, Pei C Y, Wang Q, Zhao Y, Tian S J, Li C H, Cao W Z, Chen Y L, Lei H C and Qi Y P 2023 *Appl. Phys. Lett.* **122** 172404
[19] Yan J Q, Huang Z L, Wu W D and May A F 2022 *J. Alloys Compd.* **906** 164327
[20] Zhang Z C, Feng X, Guo M H, Li K, Zhang J S, Ou Y B, Feng Y, Wang L L, Chen X, He K, Ma X C, Xue Q K and Wang Y Y 2014 *Nat. Commum.* **5** 4915
[21] Fisher M E 1962 *Philos. Mag.* **7** 173
[22] Hu C W, Gao A Y, Berggren B S, Li H, Kurleto R, Narayan D, Zeljkovic I, Dessau D, Xu S Y and Ni N 2021 *Phys. Rev. Mater.* **5** 124206
[23] Yu R, Zhang W, Zhang H J, Zhang S C, Dai X and Fang Z 2010 *Science* **329** 61
[24] Lee S H, Graf D, Min L J, Zhu Y L, Yi H M, Ciocys S, Wang Y X, Choi E S, Basnet R, Fereidouni A, Wegner A, Zhao Y F, Verlinde K, He J Y, Redwing R, Gopalan V, Churchill H O H, Lanzara A, Samarth N, Chang C Z, Hu J and Mao Z Q 2021 *Phys. Rev. X* **11** 031032
[25] Lai Y, Ke L Q, Yan J Q, McDonald R D and McQueeney R J 2021 *Phys. Rev. B* **103** 184429
[26] Islam F, Lee Y, Pajerowski D M, Oh J, Tian W, Zhou L, Yan J Q, Ke L Q, McQueeney R J and Vaknin D 2023 *Adv. Mater.* **35** 2209951